PNAS
www.pnas.org

Supplementary Information for

Divergence of the quadrupole-strain susceptibility of $YbRu_2Ge_2$; a local moment realization of electronic nematicity

Elliott W. Rosenberg, Jiun-Haw Chu, Jacob P.C Ruff, Alexander T. Hristov, and Ian R. Fisher

Elliott Rosenberg.
E-mail: erosenbe@stanford.edu

This PDF file includes:

Figs. S1 to S7
References for SI reference citations

Supporting Information (SI)

1. CEF splitting of the J=7/2 Hund's rule multiplet of $YbRu_2Ge_2$

The Hund's rule groundstate multiplet of the Yb^{3+} ion, which is characterized by a total angular momentum number J=7/2, is split by the crystal electric field (CEF) according to the effective Hamiltonian:

$$H_{CEF} = B_2^0 O_2^0 + B_4^0 O_4^0 + B_4^2 O_4^4 + B_6^0 O_6^0 + B_6^4 O_6^4 \quad [1]$$

Where O_l^m are the conventional Steven's operators (1) and B_l^m are coefficients to be determined. The resulting energy spectrum comprises 4 Kramers doublets (two doublets with Γ_6 symmetry, and two doublets with Γ_7 symmetry) and has been characterized by a combination of inelastic neutron scattering (2) and thermodynamic probes (3). The tentative spectrum of states proposed by Jeevan in (4) is Γ_6 at 91meV, Γ_7 at 32 meV, Γ_7 at 0.9 meV, and Γ_6 at 0 meV (ground state), illustrated in Fig. S1. This is the spectrum that we use to calculate the low-temperature quadrupole strain susceptibility, as described in the main text and below in Section S3. Although this is just a proposed spectrum, changing the balance of states that comprise the CEF Γ_6 groundstate and Γ_7 first excited state will affect the quadrupole moment, and will cause the 4f charge density to acquire a more pronounced 4-fold rotational symmetry, but does not change the functional form of the quadrupole strain susceptibility shown in equations 2 and 3 in the main text.

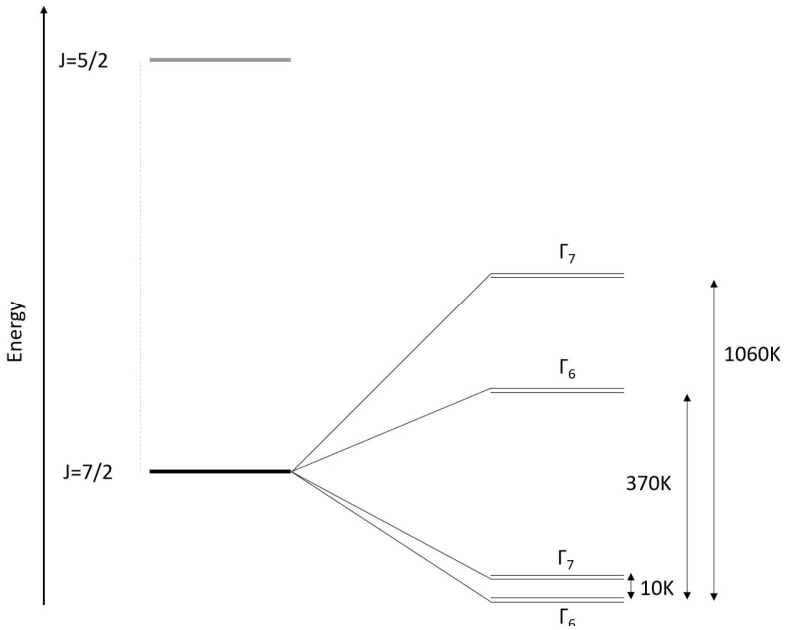

Fig. S1. $YbRu_2Ge_2$ CEF spectrum Spin-orbit coupling determines the ground state electronic mulitplet to have J=7/2, which is split by the surrounding crystalline potential to have 4 doublets, the lowest two in energy forming a quasi-quartet split by roughly 10K.

2. X-ray diffraction data for $YbRu_2Ge_2$

Low temperature, high-resolution, X-ray diffraction measurements were performed on beamline A2 at CHESS (Cornell High Energy Synchrotron Source). Splitting of the (6 0 0) Bragg peak was observed below 10.2K, with the new peaks indicative of an orthorhombic structural distortion with a B_{1g} (x^2-y^2) symmetry, the associated domain structure of which results in 4 separate peaks along the (1 1 0) and (1 -1 0) directions (5). Representative data are shown in Figures S2 and S3, taken at 12.2 K (above T_Q) and 6.6 K (below T_Q) respectively. A line cut along the (1 1 0) direction for both data sets is shown in Figure S4. The data in Figure S3 and S4 for $T < T_Q$ reveal the persistence of the central tetragonal peak, albeit with a reduced intensity, implying that some part of the illuminated volume of the crystal remains in the tetragonal state upon cooling through T_Q. Since the phase transition is characterized via heat capacity measurements to be continuous (3), this observation implies heterogeneity of either the sample temperature or of the critical temperature T_Q. Thermodynamic and transport measurements indicate a maximum spread of critical temperatures of approximately 0.5 K but at least in principle local strains due to sample mounting for the measurement can plausibly affect the critical temperature leading to a larger variation. Additional measurements would be necessary to characterize how rapidly T_Q is affected by homogeneous strains of various symmetries in order to assess whether this is the origin of the effect. To best account for this when determining the orthorhombic order parameter (shown in Figure 3 of the main paper), we obtained the position of the first moment of counts along the (1 1 0) direction (above a background threshold), that were clearly not part of the original tetragonal peak.

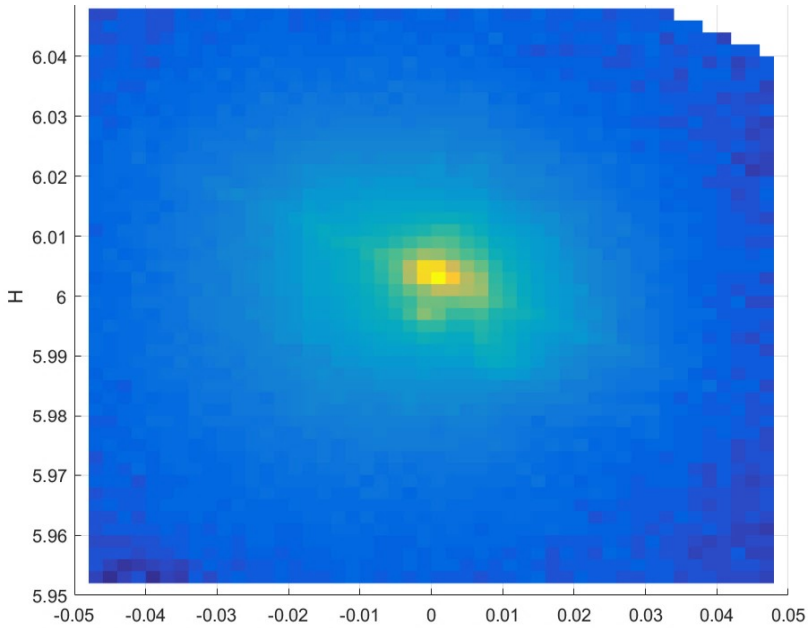

Fig. S2. Surface plot of log(intensity) at 12.2K The material is still clearly tetragonal here, although it is displaying some spread in the momentum space direction that orthorhombic domains are expected, possibly indicating critical fluctuations or a static response to unintentional strains from securing the crystal to the sample holder.

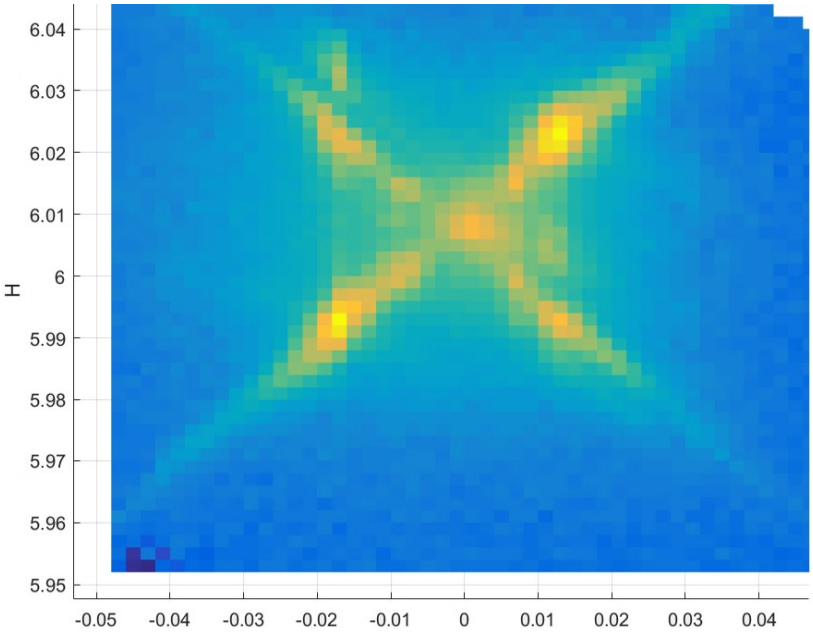

Fig. S3. Surface plot of log(intensity) at 6.6K The material is clearly orthorhombic at this temperature, displaying multiple peaks.

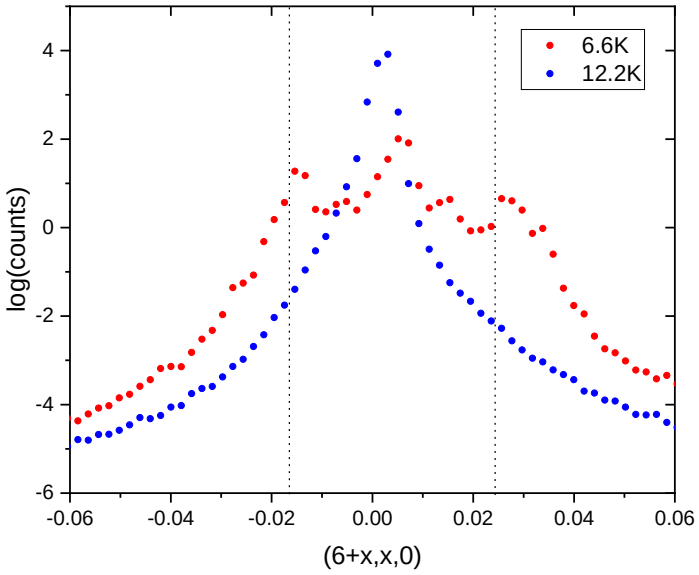

Fig. S4. Line cut of log(counts) along the (1,1,0) direction, centered at (6,0,0) The dotted lines represent where the first moment of counts was determined to be, which was normalized by the lattice parameters to determine the orthorhombic order parameter.

3. Quadrupole operators

The three relevant quadrupole operators, which correspond to the axis of the quadrupole oriented along [0 0 1] (z^2 symmetry), along [1 0 0] or [0 1 0] ($x^2 - y^2$ symmetry), and along [1 1 0] or [1 -1 0] (xy symmetry) respectively, are given by the familiar Steven's operators:

$$O_2^0 = 3J_z^2 - J(J+1) \quad [2]$$

$$O_2^2 = J_x^2 - J_y^2 = \frac{1}{2}(J_+^2 + J_-^2) \quad [3]$$

$$P_{xy} = \frac{1}{2}(J_x J_y + J_y J_x) = \frac{-i}{4}(J_+^2 - J_-^2) \quad [4]$$

In the restricted Hilbert space corresponding to the quasi-quartet CEF groundstate of $YbRu_2Ge_2$, these operators have the following matrix elements, where for convenience the basis of states is represented in the order (3/2, -1/2, -3/2, 1/2)

$$O_2^0 = \begin{bmatrix} -15 & 0 & 0 & 0 \\ 0 & -9 & 0 & 0 \\ 0 & 0 & -15 & 0 \\ 0 & 0 & 0 & -9 \end{bmatrix}$$

$$O_2^2 = \begin{bmatrix} 0 & 2\sqrt{15} & 0 & 0 \\ 2\sqrt{15} & 0 & 0 & 0 \\ 0 & 0 & 0 & 2\sqrt{15} \\ 0 & 0 & 2\sqrt{15} & 0 \end{bmatrix}$$

$$P_{xy} = \begin{bmatrix} 0 & -i\sqrt{15} & 0 & 0 \\ i\sqrt{15} & 0 & 0 & 0 \\ 0 & 0 & 0 & i\sqrt{15} \\ 0 & 0 & -i\sqrt{15} & 0 \end{bmatrix}$$

Noticing the correspondence to the Pauli spin matrices, we introduce for completeness a third, octupole, operator, that will also have finite matrix elements in this basis: $O_3^{-2} = \frac{-i}{4}(J_z(J_+^2 - J_-^2) + (J_+^2 - J_-^2)J_z)$

$$O_3^{-2} = \begin{bmatrix} 0 & -i\sqrt{15} & 0 & 0 \\ i\sqrt{15} & 0 & 0 & 0 \\ 0 & 0 & 0 & -i\sqrt{15} \\ 0 & 0 & i\sqrt{15} & 0 \end{bmatrix}$$

Inspection of these expressions reveals they can be written as tensor products of the canonical Pauli matrices and the identity, I:

$$O_0^2 = I \otimes (-3\sigma_z - 12I) \quad [5]$$

$$O_2^2 = I \otimes (2\sqrt{15}\sigma_x) \quad [6]$$

$$P_{xy} = \sigma_z \otimes (\sqrt{15}\sigma_y) \quad [7]$$

$$O_3^{-2} = I \otimes (\sqrt{15}\sigma_y) \quad [8]$$

With reference to the tensor product formula:

$$[I \otimes A, I \otimes B] = I \otimes [A, B] \quad [9]$$

and noting that constants don't affect commutation relations, the three operators O_2^0, O_2^2, and O_3^{-2} obey the canonical commutation relations. The quasi-quartet ground state can be thought of as two replicas of a pseudo-spin $\frac{1}{2}$ doublet, where the two replicas arise as a consequence of Kramer's theorem. These three operators will then serve as the effective spin operators in the three spatial dimensions of the pseudo-spin space. The quartet is split (by roughly $\Delta_0 = 10K$) due to the tetragonal point symmetry of the CEF, yielding a finite σ_z (i.e a finite O_2^0 quadrupole moment) above T_Q. Mixing of these eigenstates, as described in Figure 1 of the main text, can then yield finite quadrupole moments O_2^2 or P_{xy}.

4. Quadrupole-strain Susceptibility

Externally applied stresses cause finite strains, which in turn affect the eigenstates and eigenvalues of H_{CEF}, shifting and admixing the states described in Section S1. The magneto-elastic coupling (MEC) Hamiltonian is given by

$$H = H_{CEF} + \sum_{\Gamma_i} B_m^l \varepsilon_{\Gamma_i} Q_{\Gamma_i}$$

Where B_m^l are coefficients yet to be determined, and Γ_i are irreducible representations of the point group. Applying a non-zero stress which induces a strain ($\varepsilon_\gamma = \varepsilon_{xx} - \varepsilon_{yy}$) will induce a finite moment of $\langle O_2^2 \rangle$, which will perturbatively change the existing Hamiltonian (in the basis of the quasi-quartet) to be in the form:

$$H = H_{CEF} + B_2^2 \varepsilon_\gamma O_2^2 = I \otimes \begin{bmatrix} \Delta_0/2 & 2\sqrt{15}B_2^2\varepsilon_\gamma \\ 2\sqrt{15}B_2^2\varepsilon_\gamma & -\Delta_0/2 \end{bmatrix}$$

Diagonalizing this matrix gives a new energy gap of:

$$\Delta/2 = \sqrt{(\Delta_0/2)^2 + 60(B_2^2\varepsilon_\gamma)^2} \quad [10]$$

The thermal expectation value of the quadrupolar moment $\langle O_2^2 \rangle$ is now:

$$\langle O_2^2 \rangle = \frac{120B_2^2\varepsilon_\gamma}{\Delta} \tanh\left(\frac{\Delta}{2T}\right) \quad [11]$$

Thus the quadrupole-strain susceptibility is:

$$\chi_{Q_{B_{1g}}} = \left.\frac{dQ_{B_{1g}}}{d\varepsilon_{B_{1g}}}\right|_{\varepsilon\to 0} = \frac{60B_2^2}{T} \quad [12]$$

when $T >> \Delta_0$, and

$$\chi_{Q_{B_{1g}}} = \left.\frac{dQ_{B_{1g}}}{d\varepsilon_{B_{1g}}}\right|_{\varepsilon\to 0} = \frac{120B_2^2}{\Delta_0} \tanh\left(\frac{\Delta_0}{2T}\right) \quad [13]$$

in general.

Although in the case of the B_{2g} order parameter P_{xy} the Hamiltonian cannot be written as concisely, a similar result is still obtained:

$$\chi_{Q_{B_{2g}}} = \left.\frac{dQ_{B_{2g}}}{d\varepsilon_{B_{2g}}}\right|_{\varepsilon\to 0} = \frac{15B_{xy}}{T} \quad [14]$$

when $T >> \Delta_0$, and

$$\chi_{Q_{B_{2g}}} = \left.\frac{dQ_{B_{2g}}}{d\varepsilon_{B_{2g}}}\right|_{\varepsilon\to 0} = \frac{30B_{xy}}{\Delta_0}\tanh\left(\frac{\Delta_0}{2T}\right) \quad [15]$$

in general.

Hence both the B_{1g} and B_{2g} quadrupole strain susceptilities can be put in the form:

$$\chi_{Q_{\Gamma_i}} = \left.\frac{dQ_{\Gamma_i}}{d\varepsilon_{\Gamma_i}}\right|_{\varepsilon\to 0} = \frac{2\langle Q_{\Gamma_i}\rangle_o^2 B_{\Gamma_i}}{\Delta_0}\tanh\left(\frac{\Delta_0}{2T}\right) \quad [16]$$

Assuming no B_{1g} or B_{2g} strain is being applied, the A_{1g} quadrupole-strain susceptibility is:

$$\chi_{Q_{A_{1g}}} = \left.\frac{dQ_{A_{1g}}}{d\varepsilon_{A_{1g}}}\right|_{\varepsilon\to 0} = \frac{\langle Q_{A_{1g}}\rangle_o^2 (B_0^2)_1 \operatorname{sech}^2\left(\frac{\Delta_0}{2T}\right)}{T} \quad [17]$$

Where $\langle Q_{A_{1g}}\rangle_o = 3$

Adding in mean-field interactions of the form $H_{QQ} = K_{\Gamma_i}\langle Q_{\Gamma_i}\rangle Q_{\Gamma_i}$ will renormalize the quadrupole-strain susceptibilities to be in the form:

$$\chi_{Q_{\Gamma_i}} = \left.\frac{dQ_{\Gamma_i}}{d\varepsilon_{\Gamma_i}}\right|_{\varepsilon\to 0} = \frac{2B_{\Gamma_i}\langle Q_{\Gamma_i}\rangle_o^2 \tanh\left(\frac{\Delta_0}{2T}\right)}{\Delta_0 - 2K_{\Gamma_i}\langle Q_{\Gamma_i}\rangle_o^2 \tanh\left(\frac{\Delta_0}{2T}\right)} \quad [18]$$

For $T >> \Delta/2$ this becomes the familiar expression:

$$\chi_{Q_{\Gamma_i}} = \frac{B_{\Gamma_i}\langle Q_{\Gamma_i}\rangle_o^2}{T - \langle Q_{\Gamma_i}\rangle_o^2 K_{\Gamma_i}} \quad [19]$$

For A_{1g} this renormalizes it to become:

$$\chi_{A1g} = \frac{B_0^2\langle Q_2^0\rangle_o^2 \operatorname{sech}^2\left(\beta\left(\Delta/2 + 3K_2^0\langle O_2^0\rangle|_{\varepsilon=0}\right)\right)}{T - \langle Q_2^0\rangle_o^2 K_2^0 \operatorname{sech}^2\left(\beta\left(\Delta/2 + 3K_2^0\langle O_2^0\rangle_{\varepsilon=0}\right)\right)} \quad [20]$$

The proposed CEF quasi-quartet states (4) can be substituted in to find the actual values : $\langle Q_i\rangle_o$: $\langle O_2^0\rangle_o = 3.035$, $\langle O_2^2\rangle_o = 8.3185$, and $\langle P_{xy}\rangle_o = 3.4660$

With these values the elastoresistivity measurements can be fit to to obtain absolute values for K_i and the gap Δ and relative ratios of B_i.

5. Relation of Elastoresistivity to Quadrupole-strain Susceptibility

To show how the proportionality between the quadrupole-strain susceptibilities and the elastoresistivity coefficients is obtained, we follow Friederich and Fert (6) and extend their argument to tetragonal systems, replacing the magnetic field with strain as the source of the quadrupole moment. If we make the following assumptions that: a) the strain is perturbative, hence the quadrupole moments can be treated as impurities but the system has a infinitesimal overall quadrupole moment; b) The scattering is dominated by isotropic (in the ab plane) elastic scattering potentials $V\delta(r_i)$ at each Yb site i; c) We can use the first Born approximation to obtain the scattering rate $W_{kk'}$; and d) The conduction electrons are primarily s-wave and p-wave in character, then we can follow the argument laid out in Ref. (6).

We begin by writing down the scattering interaction between s and p wave conduction electrons and $4f$ sites originally derived by Kondo:

$$V_{scatt} = \sum_{kk'}\left[V - \frac{D}{k_f^2}\left((J\cdot k)(J\cdot k') - \frac{J(J+1)}{3}k\cdot k'\right)\right]a_{k'}^\dagger a_k' \quad [21]$$

Where D is the coefficient of the quadrupolar scattering potential from the $4f$ electrons, and V in the sum is the previously mentioned strength of the isotropic scattering potential. When this potential is plugged into Fermi's Golden rule, assuming the quadrupole term is perturbatively small, the anisotropic cross terms lead to a resistivity ratio directly from Ref. (6), Equation 3:

$$\frac{\rho_i^Q}{\rho_0} = \frac{2D}{3V}\left(\langle J_i^2\rangle - \frac{J(J+1)}{3}\right) \quad [22]$$

Where i is the direction of the current, and ρ_0 is the resistivity due to the isotropic scattering potential (isotropic only in the ab plane in the case of $YbRu_2Ge_2$)

Thus:

$$\frac{\rho_x^Q - \rho_y^Q}{2\rho_0} = \frac{D}{3V}\left(\langle J_x^2\rangle - \langle J_y^2\rangle\right) = \frac{D}{3V}\langle O_2^2\rangle \quad [23]$$

Because inelastic scattering should only be dependent on the magnitude of the gap and matrix elements like $\langle|Q_i|\rangle^2$, its B_{1g} component induced by strain should be close to zero. Similarly the anisotropic part of the Kondo scattering should be close to zero, as there is no reason to suggest there are quadrupolar aspects of the coupling of conduction electrons to the magnetic aspects of the $4f$ sites. Thus, taking the appropriate strain derivatives (in this case, with respect to $\varepsilon_{xx} - \varepsilon_{yy}$), we find that the elastoresistivity associated with scattering from the $4f$ orbital is directly proportional (with a temperature independent proportionality coefficient) to the B_{1g} quadrupole-strain susceptibility.

$$\left.\frac{\frac{\partial(\rho_{4f}^{xx} - \rho_{4f}^{yy})}{\rho_{4f}^0}}{\partial\varepsilon_{B1g}}\right|_{\varepsilon\to 0} \approx \frac{D}{3V}\frac{\partial\langle O_2^2\rangle}{\partial\varepsilon_{B1g}} \propto \chi_{B1g} \quad [24]$$

Several scattering processes contribute to the resistivity of $YbRu_2Ge_2$. Assuming validity of Matthiessen's rule, $\rho_{YbRu2Ge2} = \rho_{imp} + \rho_{e-ph} + \rho_{e-e} + \rho_{4f}$ where ρ_{imp} arises from impurity scattering, ρ_{e-ph} from electron-phonon interactions, ρ_{e-e} from electron-electron scattering, and ρ_{4f} is defined above. At least in principle, each of these terms can have an associated elastoresistivity; the expression derived in Eq. 24 above relates only to the $4f$ part. Contributions to the resistivity and elastoresistivity arising from ρ_{imp}, ρ_{e-ph} and ρ_{e-e} can be subtracted by considering a non-magnetic analog that has the same crystal structure, the same band structure and a similar impurity concentration. YRu_2Ge_2 (note that Y = Yttrium, different to Ytterbium Yb) potentially provides such a non-magnetic analog. Such a subtraction would then yield,

$$\frac{\frac{\partial(\rho_{4f}^{xx} - \rho_{4f}^{yy})}{\rho_{4f}^0}}{\partial\varepsilon_{B1g}} \approx \frac{\frac{\partial(\rho_{YbRu_2Ge_2}^{xx} - \rho_{YbRu_2Ge_2}^{yy})}{\rho_{YbRu_2Ge_2}^0 - \rho_{YRu_2Ge_2}^0} - \frac{\partial(\rho_{YRu_2Ge_2}^{xx} - \rho_{YRu_2Ge_2}^{yy})}{\rho_{YbRu_2Ge_2}^0 - \rho_{YRu_2Ge_2}^0}}{\partial\varepsilon_{B1g}} \quad [25]$$

where superscripts '0' refer to zero strain conditions.

The unstrained resistivity of YRu_2Ge_2, $\rho_{YRu2Ge2}^0$, is found to be almost an order of magnitude smaller than that of $YbRu_2Ge_2$ (see Figure 3 in the main paper). Furthermore, normal metals far from any electronic instabilities, typically exhibit very small elastoresistivities. Hence, we can safely make the approximation that:

$$\frac{\frac{\partial(\rho_{4f}^{xx} - \rho_{4f}^{yy})}{\rho_{4f}^0}}{\partial\varepsilon_{B1g}} \approx \frac{\frac{\partial(\rho_{YbRu_2Ge_2}^{xx} - \rho_{YbRu_2Ge_2}^{yy})}{\rho_{YbRu_2Ge_2}^0}}{\partial\varepsilon_{B1g}} \propto \chi_{B1g} \quad [26]$$

Hence elastoresistivity will be a direct measure of the quadrupole-strain susceptibility given these conditions.

6. Linearity of the B_{1g} elastoresistivity

An effective way to show that the elastoresistivity is linear in strain while using the AC technique that we describe in the main paper is to perform these measurements for a variety of offset bias strains. In Fig. S5 we show data for the B_{1g} response for measurements performed with an AC amplitude corresponding to a peak-to-peak voltage applied to the PZT stack of 40 volts, with a simultaneous DC bias voltage of 0V, -250V and + 250V in the temperature range from 6 to 20 K. Over this temperature range, these offset voltages correspond to DC strain offsets (relative to 0V) of approximately 0, -0.021%, and 0.029% . As can be seen by inspecting the figures, in the temperature range above T_Q, the data almost perfectly line up, demonstrating the absence of any significant non-linear response.

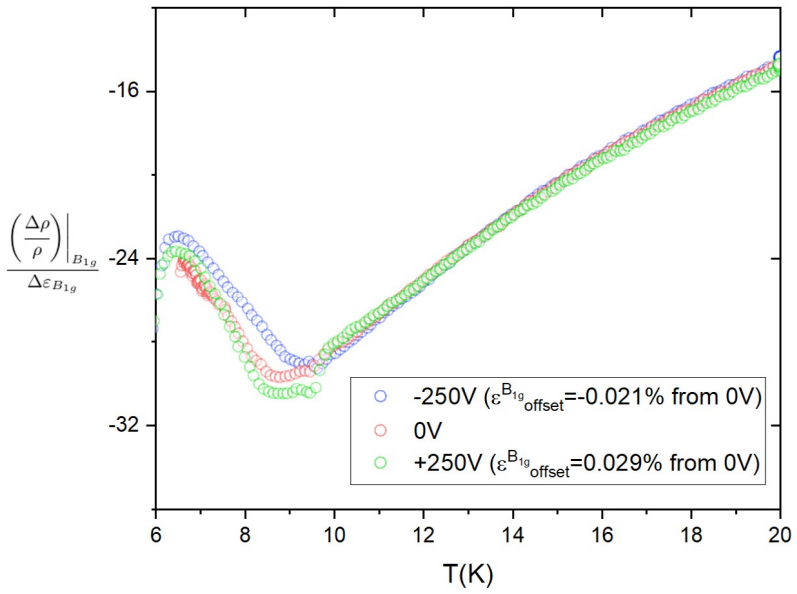

Fig. S5. Strain dependence of the B_{1g} elastoresistivity response The B_{1g} quadrupole-strain susceptibility displays little sensitivity to tuning B_{1g} offset strains above the quadrupolar phase transition indicating this channel is dominated by linear behavior, and hence $\left(\frac{\Delta\rho}{\rho}\right)_{B_{1g}}/\Delta\varepsilon_{B_{1g}}$ provides a good measure of the linear elastoresistivity coefficients for this symmetry channel, m_{11}-m_{12}

7. Non-linearity of the A_{1g} elastoresistivity

In contrast to the case of B_{1g} response, the in-plane A_{1g} response $\frac{\rho_{xx}+\rho_{yy}}{\rho_0}$ exhibited a striking non-linearity. Fig. S6 shows the response for measurements performed with an AC amplitude corresponding to a peak-to-peak voltage applied to the PZT stack of 40 volts, with a simultaneous DC bias voltage of 0V, -250V and + 250V in the temperature range from 6 to 20 K. Over this temperature range, these offset voltages correspond to DC strain offsets (relative to 0V) of approximately 0, -0.021%, and 0.029% . The sample was oriented on the PZT stack such that the crystal experienced a combination of A_{1g} and B_{1g} strains for Fig. S6 , and A_{1g} and B_{2g} strains for Fig. S7. As can be seen, there is a striking difference between the measurements, indicating the presence of a substantial non-linear A_{1g} elastoresistivity in response to B_{1g} symmetry strains.

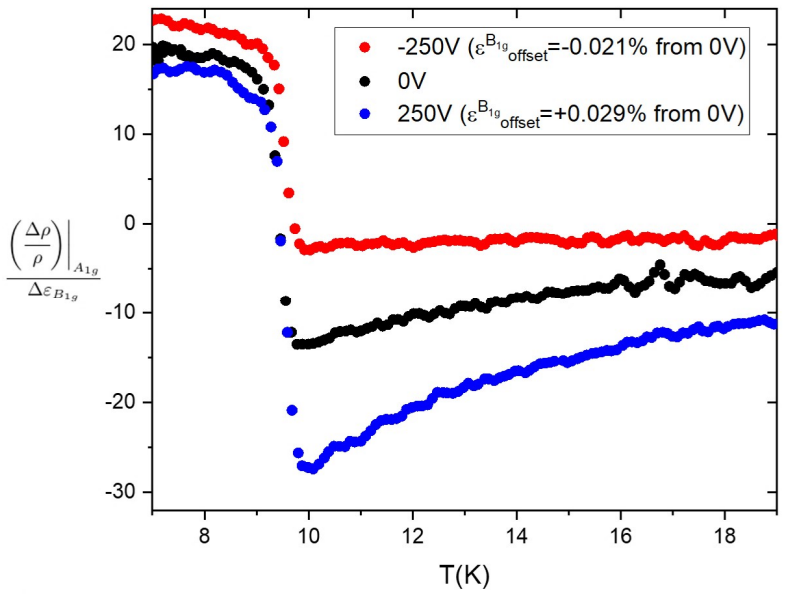

Fig. S6. Non-linearity of the A_{1g} response with respect to B_{1g} strain. The A_{1g} quadrupole-strain susceptibility displays striking sensitivity to tuning offset B_{1g} strains above the quadrupolar phase transition.

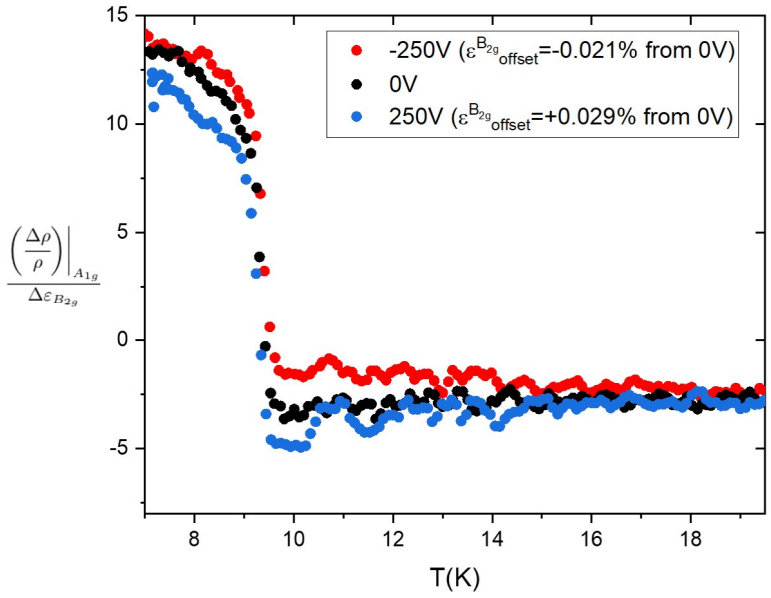

Fig. S7. Non-linearity of the A_{1g} response with respect to B_{2g} strain. The A_{1g} quadrupole-strain susceptibility displays small sensitivity to tuning offset A_{1g} and B_{2g} strains above the quadrupolar phase transition.

Although the A_{1g} response is not the main subject of this paper, we outline below the origin of this effect, making particular reference to how this shows up in an AC measurement.

To second order in strain, a crystal that experiences both A_{1g} and B_{1g} symmetry strains can experience an A_{1g} elastoresistance response given by

$$\left(\frac{\Delta\rho}{\rho_0}\right)_{A_{1g}} = m^{A_{1g}}_{A_{1g}}\varepsilon_{A_{1g}} + m^{A_{1g},A_{1g}}_{A_{1g}}[\varepsilon_{A_{1g}}]^2 + m^{B_{1g},B_{1g}}_{A_{1g}}[\varepsilon_{B_{1g}}]^2 \quad [27]$$

Where we are following the notation used in Ref.[(7)]. The linear term proportional to $\varepsilon_{A_{1g}}$ is allowed by symmetry as well as quadratic terms proportional to $\varepsilon^2_{B_{1g}}$.

Since the AC Elastoresistivity method used for these measurements locks in to the response at the frequency ω at which the strain is applied, it is useful to write the strains out as a combination of DC offset strains (arising for example from thermal expansion mismatches and glue strains, as well as intentional bias strains as mentioned previously) and AC applied strains:

$$\varepsilon_i^{tot} = \varepsilon_i^{DC} + \varepsilon_i^{AC}\cos\omega t \quad [28]$$

Where i represents the symmetry channel and the amplitude of the AC term depends on the voltage waveform applied to the piezo. Substituting into Eq. 27 and focusing on the amplitude of the signal that will be locked into at frequency ω:

$$\left(\frac{\Delta\rho}{\rho_0}\right)^{AC}_{A_{1g}} = m^{A_{1g}}_{A_{1g}}\varepsilon^{AC}_{A_{1g}} + 2m^{A_{1g},A_{1g}}_{A_{1g}}\varepsilon^{DC}_{A_{1g}}\varepsilon^{AC}_{A_{1g}} + 2m^{B_{1g},B_{1g}}_{A_{1g}}\varepsilon^{DC}_{B_{1g}}\varepsilon^{AC}_{B_{1g}} \quad [29]$$

Thus we can expect both a linear and non-linear contribution to the signal, with the strength of the non-linear part determined by both the amount of offset strain and the quadratic coefficient of that channel.

A similar difference in non-linear elastoresistivity coefficients was recently observed for the underdoped Fe-based superconductor, $Ba(Fe_{0.975}Co_{0.025})_2As_2$ (7). In that material, the nematic transition occurs in the B_{2g} symmetry channel and the quantity $m^{B_{2g},B_{2g}}_{A_{1g}}$ exhibits a divergence. In the present case, $YbRu_2Ge_2$ undergoes a nematic transition in the B_{1g} symmetry channel, and the quantity $m^{B_{1g},B_{1g}}_{A_{1g}}$ appears to grow very large. Both results highlight the role played by nematic (quadrupole) fluctuations in affecting the isotropic properties of materials . In the case of $YbRu_2Ge_2$, the observation of a large $m^{B_{1g},B_{1g}}_{A_{1g}}$ adds further evidence to our conclusion that the quadrupole-strain susceptibility is large in the B_{1g} channel but small in the B_{2g} channel.

8. Focused Ion Beam parameters

The instrument used to etch the samples was an FEI Helios NanoLab 600i DualBeam FIB/SEM, containing both a focused Ga+ ion beam ("Tomahawk") and a high resolution field emission scanning electron ("Elstar") column. Combined with advances in patterning, scripting, and a suite of accessories, these features make milling, imaging, analysis, and sample preparation down to the nanoscale possible.

A 65 nA ion current was used to etch through the samples. Gallium implantation is expected to affect a depth of less than 100 nm from the surface roughly, which is inconsequential for the bulk resistivity measurements that were performed.

9. Crystal Growth and Measurement Details

Single crystals of $YbRu_2Ge_2$ were grown using an unseeded flux method, with Indium being the flux and the other precursors added in stoichiometrically. The flux ratio was varied from 96-98%, with 97.5% found to produce both the largest size individual crystals and also the greatest yield. To help ensure inclusion of the high-melting point Ru into the melt, the elemental Ru and Ge precursors were arc-melted in a mono-arc furnace. The elements were then combined into an alumina crucible, which was sealed inside a Ta crucible to prevent oxidation and to contain the flux. The crucibles were heated to a max temperature of 1450K for 6-12 hours, and then cooled to 1200K at approximately 4K/hour. The alumina crucibles were then sealed in quartz and spun in a centrifuge at 400K to remove the Indium flux from the crystals. The resulting crystals were etched in HCl acid for several months until they were easily cleaveable.

For transport and elastoresistivity measurements, current and voltage contacts were made to the sample by connecting gold wires to the sample using Epotech H-20E silver paste. Typical bar dimensions for samples in elastoresistivity measurements were 200-400μm in length, by 70-120μm in width. Samples were glued using Angstrom Bond to Si substrates, which were then bonded to the center of a side of a Piezomechanick 5x5x9 mm PZT piezoelectric stack (Piezomechanik PSt150/5x5/7 cryo 1) in the appropriate orientation using Devcon 5-Minute Epoxy. Uncertainty in alignment with respect to the crystal axes was estimated to be less than 2 degrees. The PZT stack was mounted on a thermally anchored probe in a helium flow cryostat.

AC Elastoresistivity measurements were applied using a 1.6Hz 50V rms sinusoidal excitation to the PZT while simultaneously driving a 5 mA rms current through the sample at 107 Hz, sourced by a Keithley 6221 DC and AC current source.

The signal was first measured by a SRS830 lock-in amplifier (LIA) with a time constant < 30ms referenced to 107 Hz, and the output of that LIA is measured by a second LIA with a time constant of > 3s referenced at 1.6Hz to detect the elastoresisitivity signal. Care was taken to ensure the phase of the output signal was properly accounted for. Strain transmission was measured from the piezo surface to the top surface of the Si where the samples were glued, and was determined to be roughly 50% and essentially temperature independent from 4K to 100K. This was taken into account in determining the magnitude of the elastoresistivity coefficients.

References

1. Morin P, Schmitt D (1990) Quadrupolar interactions and magneto-elastic effects in rare earth intermetallic compounds **Handbook of Ferromagnetic Materials, Vol. 5 1990, 1-132**
2. Jeevan HS, Adroja DT, Hillier AD Hossain Z, Ritter C, Geibel C (2011) Muon spin relaxation and neutron diffraction investigations of quadrupolar and magnetically ordered states of $YbRu_2Ge_2$ **Phys Rev B 84, 184405**
3. Jeevan HS, Geibel C, Hossain Z (2006) Quasiquartet crystal-electric-field ground state with possible quadrupolar ordering in the tetragonal compound $YbRu_2Ge_2$ **Phys Rev B 73 020407(R)**
4. Jeevan HS (2010) Crystal Growth and Investigation of $CeCu_2Si_2$ and $YbRu_2Ge_2$: Competition/Co-existence of Superconducting, Dipolar and Quadrupolar order **core.ac.uk**
5. Blomberg EC et al (2012) Effect of tensile stress on the in-plane resistivity anisotropy in $BaFe_2As_2$ **Phys. Rev. B 85, 144509**
6. Friederich A and Fert A (1974) Electron Scattering by the Electronic Quadrupole Moment of Rare-Earth Impurities **Phys. Rev. Lett. 33 1214**
7. Palmstrom JC et al (2017) Critical divergence of the symmetric (A_{1g}) nonlinear elastoresistance near the nematic transition in an iron-based superconductor **Phys Rev B 96.205133**